Processing Design of Miniature Casting Incorporating Stereolithography Technologies

Pei-Hsing Huang, Wei-Ju Huang

Abstract—Investment casting is commonly used in the production of metallic components with complex shapes, due to its high dimensional precision, good surface finish, and low cost. However, the process is cumbersome, and the period between trial casting and final production can be very long, thereby limiting business opportunities and competitiveness. In this study, we replaced conventional wax injection with stereolithography (SLA) 3D printing to speed up the trial process and reduce costs. We also used silicone molds to further reduce costs to avoid the high costs imposed by photosensitive resin.

Keywords—Investment casting, stereolithography, wax molding, 3D printing.

I. INTRODUCTION

CURRENT considerations in gating system design of investment casting include production efficiency, precision, and a good surface finish [1]. During the initial stage of casting blanks, new production lines tend to be developed through trial and error [2]. Thus, the flow behavior and solidification of molten metal are hard to predict. This increases the likelihood of shrinkage and pore formation in casts [3]. Combining stereolithography and casting technology, this study used a laser beam and photosensitive resin material to create wax molds for investment casting. This technique is already being widely applied in Japan, Europe, and America for the production of samples, performing trial assembly, and testing functions [4], [5]. Research has shown that employing mold flow analysis to design casting schemes can greatly increase yields [6]. Using the aforementioned technologies, we examined the characteristics and defect formation of investment casting for a miniature blade casting. Via the designs of SLA printing parameters, we improve the quality of wax patterns, increase efficiency in design and production, and save the costs of injection molding.

II. EXPERIMENTAL AND NUMERICAL METHODS

A. Gating Systems and Process Parameter Design

Existing wax molding techniques can produce several types of components in one piece or components that have thin walls and complex shapes or are difficult to machine with good dimensional accuracy and surface finishes. Using SolidWorks software, we created a miniature turbine blade with thin walls

Pei-Hsing Huang (Professor) is with the National Pingtung University of Science and Technology, Pingtung, Taiwan (corresponding author, phone: +886-8-7703202; fax: +886-8-7740142; e-mail: phh@mail.npust.edu.tw).

Wei-Zu Huang is a graduate student at the National Pingtung University of Science and Technology, Pingtung, Taiwan (phone: +886-8-7703202; fax: +886-8-7740142; e-mail: king19950222x@gmail.com).

as the subject component of this study. The blades possess an outside diameter of 30 mm and the thickness of the blades was 0.6 mm (as shown in Fig. 1). We experimented on various pattern trees to optimize the processing design (as shown in Fig. 2). Table I presents the experiment parameters of the casting process.
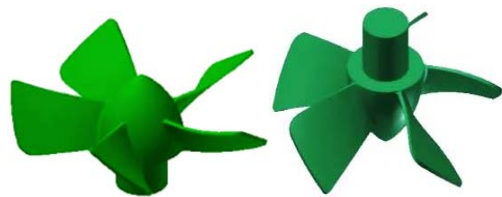

Fig. 1 Configuration of turbine blade

TABLE I
EXPERIMENT PARAMETERS OF CASTING PROCESS

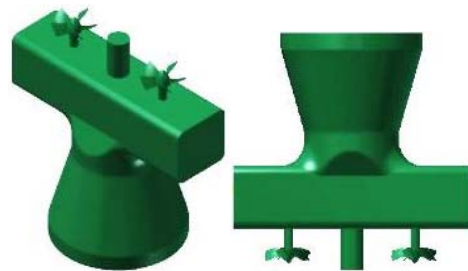|	Exp.1	Exp.2	Exp.3
Material		SUS304	
$T_{ceramic}$ (°C)		1200	
$T_{casting}$ (°C)	1500	1600	1700
Ceramic shell material		Zircon(Zr) sand	
δ (mm)		5.5	
Mesh number		2,989,440	
$t_{pouring}$ (sec)		6	
Cooling		Air	

Fig. 2 Design of pouring system

B. Fundamental Theory of Mold Flow Analysis

The thermal analysis of metal castings during the solidification process is a transient thermal analysis. In the temperature field of this analysis, the function of time is t, and the function of space is Ω. The time and space domains cannot be coupled directly, so partial separation is needed to establish the finite element scheme.

The thermal conduction mode of the three-dimensional temperature field is [7]-[9]:

World Academy of Science, Engineering and Technology
International Journal of Aerospace and Mechanical Engineering
Vol:11, No:8, 2017

$$\frac{\partial}{\partial x}(k\frac{\partial T}{\partial x}) + \frac{\partial}{\partial y}(k\frac{\partial T}{\partial y}) + \frac{\partial}{\partial z}(k\frac{\partial T}{\partial z}) + q_v = \frac{\partial}{\partial t}(\rho H) \tag{1}$$

Thermal conduction has three types of boundary conditions:
First type of boundary condition:

$$\Gamma_1 = T = T_0 \tag{2}$$

Second type of boundary condition:

$$\Gamma_2 : (k\frac{\partial T}{\partial x}n_x) + (k\frac{\partial T}{\partial y}n_y) + (k\frac{\partial T}{\partial x}n_x) = q \tag{3}$$

Third type of boundary condition:

$$(k\frac{\partial T}{\partial x}n_x) + (k\frac{\partial T}{\partial y}n_y) + (k\frac{\partial T}{\partial z}n_z) = h(T_a - T) \tag{4}$$

1. Continuity Equation

The following equation describes the conservation of mass in liquid metal, wherein in a given area, any increase in fluid mass is equal to the mass flowing from the surrounding areas into the variable area.

$$\frac{\partial \rho}{\partial t} + \frac{\partial(\rho u_x)}{\partial x} + \frac{\partial(\rho u_y)}{\partial y} + \frac{\partial(\rho u_z)}{\partial z} = 0 \tag{5}$$

2. Energy Equation

The equation represents that the change in the total energy within an area equals the summation of work done by the forces applied to the area and the energy transferred into the area.

$$\frac{de}{dt} + P\frac{d}{dt}(\frac{1}{\rho}) = \frac{1}{\rho}div\,(\lambda\,gradT\,) + \frac{\varphi}{\rho} \tag{6}$$

3. Navier-Stoke (N-S) Equation

According to Newton's second law of motion, the equation of motion for viscous fluids that is derived is the mathematical expression of the law of conservation of momentum.

$$\rho\frac{du_x}{dt} = \rho F_x - \frac{\partial P}{\partial x} + \frac{\partial}{\partial x}[\mu(2\frac{\partial u_x}{\partial x} - \frac{2}{3}div\vec{u})] + \frac{\partial}{\partial y}[\mu(\frac{\partial u_x}{\partial y} + \frac{\partial u_y}{\partial x})] + \frac{\partial}{\partial z}[\mu(\frac{\partial u_z}{\partial x} + \frac{\partial u_x}{\partial z})] \tag{7}$$

$$\rho\frac{du_y}{dt} = \rho F_y - \frac{\partial P}{\partial y} + \frac{\partial}{\partial y}[\mu(2\frac{\partial u_y}{\partial y} - \frac{2}{3}div\vec{u})] + \frac{\partial}{\partial z}[\mu(\frac{\partial u_y}{\partial z} + \frac{\partial u_z}{\partial y})] + \frac{\partial}{\partial x}[\mu(\frac{\partial u_x}{\partial y} + \frac{\partial u_y}{\partial x})] \tag{8}$$

$$\rho\frac{du_z}{dt} = \rho F_z - \frac{\partial P}{\partial z} + \frac{\partial}{\partial z}[\mu(2\frac{\partial u_z}{\partial z} - \frac{2}{3}div\vec{u})] + \frac{\partial}{\partial x}[\mu(\frac{\partial u_z}{\partial x} + \frac{\partial u_x}{\partial z})] + \frac{\partial}{\partial y}[\mu(\frac{\partial u_y}{\partial z} + \frac{\partial u_z}{\partial y})] \tag{9}$$

4. Turbulent Flow Equation

The following Reynolds-averaged N-S equations involve averaging the continuity of turbulent flow motion and the N-S equation once in order to produce a time-averaged equation of motion for turbulent flow.

$$\rho\frac{du_y}{dt} = \rho F_y - \frac{\partial P}{\partial y} + \frac{\partial}{\partial y}[\mu(2\frac{\partial u_y}{\partial y} - \frac{2}{3}div\vec{u})] + \frac{\partial}{\partial z}[\mu(\frac{\partial u_y}{\partial z} + \frac{\partial u_z}{\partial y})] + \frac{\partial}{\partial x}[\mu(\frac{\partial u_x}{\partial y} + \frac{\partial u_y}{\partial x})] \tag{10}$$

5. Volume of Fluid (VOF) Function

The SOI-VOF function replaces the tagged particles in MAC calculations to confirm the location of the free fluid surface.

$$\frac{\partial F}{\partial t} + u\frac{\partial F}{\partial x} + v\frac{\partial F}{\partial y} + w\frac{\partial F}{\partial z} = 0 \tag{11}$$

In (1)-(11), ρ represents density (kg/m³), u denotes velocity vector (m/s), P stands for pressure (Pa), T means temperature (°C), k denotes thermal conductivity (W/m·K), F is the volume fraction (e.g., the VOF), Fx represents particle weight (body force) in x-component, μ denotes dynamic viscosity (mPa·s).

III. Results and Discussion

A. Results of Mold Flow Analyses

To prevent defects such as shrinkage cavities and pores within the turbine blade castings, we investigated the influence of temperature variations on the castings. Shrinkage cavities did not change significantly and mostly appeared in the sprue cup, which did not affect the quality of the finished castings (as shown in Fig. 3). The occurrence of shrinkage pores reduced as the temperature increased (as shown in Fig. 4). Shrinkage pore incidence was greater at 1500 °C, and as the temperature increased, the castings performed at 1600 °C and 1700 °C show that shrinkage pore incidence in the center of the sprue cup and around the blades had already greatly decreased by 1700 °C. This demonstrates that temperature indeed influences the casting quality in simulations.
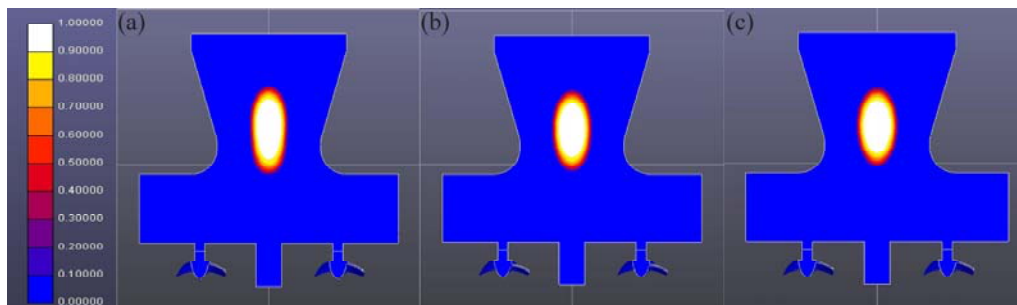

Fig. 3 (a)-(c) The probabilities of shrinkage formation at 1,500 °C, 1,600 °C, and 1,700 °C

World Academy of Science, Engineering and Technology
International Journal of Aerospace and Mechanical Engineering
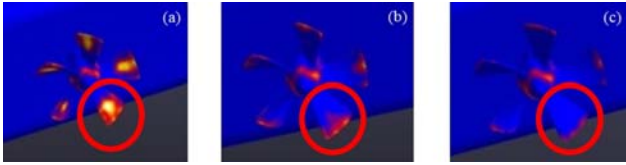Vol:11, No:8, 2017

Fig. 4 (a)-(c) The changes in shrinkage pores at 1500 °C, 1600 °C, and 1700 °C

B. Silicon Mold Process

The main feature of 3D printing with stereolithography is that it can create large, geometrically-complete products with good surface finishes within a short amount of time [10]. However, photosensitive resin is expensive and requires supporting materials during production; post-treatment is also needed to clean the product afterwards. To reduce experiment costs and the trouble of cleaning, we incorporated silicone molds [11], [12]. Stereolithography is only needed to make one product. Then, silicone molds can be used for the mass production of wax molds. Fig. 5 shows the silicone mold production process and displaying the completed mold cavity. Fig. 6 exhibits the solidified product of wax injection.

Fig. 5 Creation of silicon mold for wax injection

Fig. 6 Product of wax injection

C. Casting Results with Different Stereolithography Materials

1. ABS Photosensitive Resin

ABS resin is transparent and has a density of 1.04~1.06 g/cm^3 and printable layer thickness of 0.025 mm to 0.05 mm. This material has a low expansion rate and prints smooth surfaces. However, in reality, it can cause more severe shell breakage than wax resin (as shown in Fig. 7). The resulting castings similarly had varying defects. This casting was made at a casting temperature of 1700 °C.

2. Wax Resin

Wax resin is dark green and has a density of 0.98 g/cm^3 and printable layer thickness of 0.025 mm to 0.05 mm. The was resin possesses a lower melting point, ~400 °C, than a ABS photosensitive resin. Its actual casting results are better than those of ABS (as shown in Fig. 8). The features of this material are that it can be burnt completely and that it has a low thermal expansion coefficient. Again, this casting was made at a casting temperature of 1700 °C.

3. Results of Castings

We conducted a comprehensive assessment of the pouring schemes with regard to field stability, ventilation/trapped air, directionality of solidification, and probability of defect formation, based on the numerical simulations. The resulting casting tree produced from the wax patterns of Figs. 7 and 8 are presented in Figs. 9 (a) and (b).
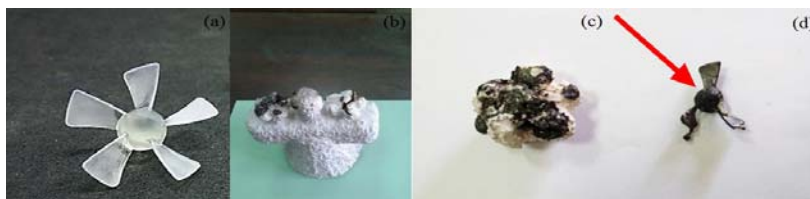

Fig. 7 (a)-(d) Printed ABS resin component, completed shell casting, and product of casting at a temperature of 1700 °C
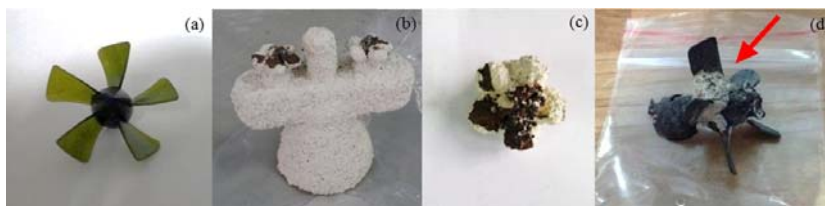

Fig. 8 (a)-(d) Printed wax resin product, completed shell casting, and product of casting at a temperature of 1700 °C
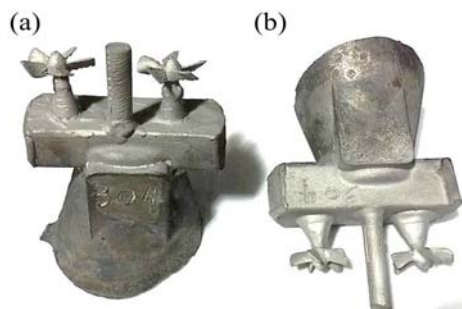
World Academy of Science, Engineering and Technology
International Journal of Aerospace and Mechanical Engineering
Vol:11, No:8, 2017

Fig. 9 Product cast directly after 3D printing (a) and product cast using silicone mold after 3D printing (b)

IV. CONCLUSION

This study used AnyCasting software to simulate and analyze the casting of a miniature turbine blade. Via simulation, we located the defects and optimized the casting process accordingly to reduce the defects and enhance casting quality.

The primary conclusions of this study were as follows:

1. Casting temperature influences defect formation. Increasing the casting temperature increases the shrinkage rate of the liquid metal, which increases the amount of shrinkage. To reduce the shrinkage and oxidation of the liquid metal, we kept the casting temperature to between 50 °C and 150 °C. The liquidous temperature of the 304-stainless steel used in this study was 1449 °C. The manufacturer suggested casting temperatures of 1600±100 °C for our study. Experiments indicated that the best casting temperature was 1700 °C; the resulting casting contained less shrinkage porosity than the castings made at other temperatures.

2. The simulation data indicated more shrinkage pores in the turbine blades. This is because the outer edges of the blades cool down first, followed by the bases of the blades near the shaft. As a result, the casting could not solidify properly.

3. Conducting analysis before opening the mold to derive the casting, cooling, flow field, temperature, and pore distribution can provide reference for defect and design improvement. This will prevent issues during mold development and effectively reduce product development time, thereby enabling investment casting to produce fine and precision components.

4. Stereolithography can create high-precision models for casting reference, which eliminates the need for the wax injection and pattern assembly processes and thus enables manufacturers to accelerate mold production and reduce costs.

5. Silicone molds can cut down on experiment costs and resolve the issue of photosensitive resin being expensive.

ACKNOWLEDGMENT

REFERENCES

[1] P. H. Huang, Y. T. Chen, B. T. Wang, "An effective method for separating casting components from the runner system using vibration-induced fatigue damage," *International Journal of Advanced Manufacturing Technology*, vol. 74, pp. 1275-1282, 2014.

[2] J. K. Kuo, P. H. Huang, H. Y. Lai, J. R. Chen, "Optimal gating system design for investment casting of 17-4PH stainless steel enclosed impeller by numerical simulation and experimental verification," *International Journal of Advanced Manufacturing Technology*, DOI 10.1007/s00170-017-0198-0, 2017.

[3] P. H. Huang, W. J. Wu, C. H. Shieh, "Numerical simulations of low pressure die-casting for A356 aluminum rim," *Materials Science Forum*, vol. 893, pp. 276-280, 2017.

[4] X. W. Zong, Y. X. Liu, G. Wei, Y. Q. Wang, B. H. Lu, "Investment Casting Processing Based on Stereoligraphy," *Journal of Xi'an Jiaotong University*, vol.41, no.1, 2007.

[5] D. M. Yu, X. J. Li, "Analysis for Precision Based on Stereo Lithography Apparatus Rapid Prototyping", *Henan Polytechnic Institute*, vol.43, no. 8, 2015.

[6] J. K. Kuo, P. H. Huang, M. J. Guo, "Removal of CrMo alloy steel components from investment casting gating system using vibration-excited fatigue failure," *International Journal of Advanced Manufacturing Technology*. vol. 89, pp. 101–111, 2017.

[7] User manual of Anycasting. version 6.0.

[8] P. H. Huang, M. J. Guo, "A study on the investment casting of 17-4PH stainless steel helical impeller of centrifugal pump", *Materials Research Innovations*, vol. 19, pp. S9, 77-81, 2015.

[9] P. H. Huang, J. Y. Luo, S. C. Hung, C. J. Lin, H. H. Cheng, "Optimal pouring system design for investment casting of cladding thin-plate heater using metallic mold flow analyses," *Applied Mechanics and Materials*, vol. 627, pp. 46-49, 2014.

[10] F. Gao, W. Tan, "SLA rapid casting resin mold investment casting," Qingan Group Co., Shanxi Hengtong Intelligent Machine Co, assembly documents, 2011.

[11] P. H. Huang, W. J. Wu, C. H. Shieh, "Compute-aided design of low pressure die-casting process of A356 aluminum wheels," *Applied Mechanics and Materials*, vol. 864, pp. 173-178, 2017.

[12] P. H. Huang, C. J. Lin, "Computer-aided modeling and experimental verification of optimal gating system design for investment casting of precision roto*r, International Journal of Advanced Manufacturing Technology*, vol. 79, pp. 997-1006, 2015.

Pei-Hsing Huang is a professor at the National Pingtung University of Science and Technology, Pingtung, Taiwan. His academic expertise is in the area of mechanical manufacturing, including investment casting, laser sintering, and molecular dynamics. He is the senior member of International Association of Computer Science and Information Technology (IACSIT) and South Asia Institute of Science and Engineering (SAISE). He is the director member of International Society of Mechatronic Engineering (ISME) in Taiwan. He also is the member of American Chemical Society (ASC), World Academy of Science, Engineering and Technology (WASET), the Royal Society of Chemistry (RSC), and the Science and Engineering Institute (SCIEI). Wei-Zu Huang is a graduate student in the department of M.E. at the National Pingtung University of Science and Technology, Pingtung, Taiwan.